Chapter 4

Modelling and Simulation Study of Ultrasonic Vibration-Assisted Grinding of AISI D2 Tool Steel with Single Alumina Abrasive Grit

4 Introduction

In the precision fabrication industries, ultrasonic vibration assisted grinding is widely utilized for the finishing of "difficult-to-cut" materials due to its intermittent cutting mechanism and brittle-to-ductile mode machining. In this chapter, a 2D finite element model (FEM) of single grit ultrasonic vibration assisted dry grinding (UVADG) and conventional dry grinding (CDG) of AISI D2 steel has been developed, which taken into account the influence of longitudinal ultrasonic vibration on the workpiece with variable downfeed. The effects of ultrasonic vibration and downfeed on the chip formation mechanism, temperature field, grinding force and equivalent stress and strain were evaluated by analytical and simulation methods. Also, to enhance the accuracy of the simulated results, author has performed a mesh sensitivity analysis. The results show that the formation of the grinding chips under UVADG is much shorter and straighter than CDG mode at all respective downfeed. The validation experiment compared the simulated and experimental grinding force in both grinding modes to verify the reliability of the FEA results. The validation results demonstrate that the FEA model can accurately describe the single grit UVADG and CDG grinding. At each downfeed, the CDG mode has generated a larger equivalent plastic strain than the UVADG mode, resulting in a higher thermo-mechanical load on the workpiece. According to the findings, UVADG mode has least plastic damage on the ground surface, which may improve the surface integrity of the ground component. The available literature cited in Chapter 2 indicated that though several past research have concentrated on ultrasonic vibration assisted grinding (UVAG), the chip formation mechanism, temperature field, and effect of stress and strain on the "difficult-to-

cut" materials have not yet been investigated in detail. Macroscopic results are typically formed of microscopic outcomes. In UVADG, the workpiece material is removed by the discontinuous micro-cutting action of the abrasive grits, which is the summation of the microscopic effects of individual abrasive grits [190]. For that reason, it is crucial to examine the synergy between single abrasive grit and the surface of the workpiece for a more proper understanding of the mechanism of UVADG.

From the preceding review on the fundamental studies of the conventional grinding process, although substantial work has been performed on the examination of single grit conventional grinding process. The research gaps identified as summarized below. The research work in UVAG with a single abrasive grit for engineering materials is almost nil. Therefore, in order to thoroughly understand the chip formation mechanism, temperature field, equivalent stress and strain into "difficult-to-cut" material like AISI D2 tool steel under UVAG. Author have planned their experimentations with a single alumina abrasive grit. Furthermore, analytical, and simulated models in CDG and UVADG modes are likely to permit the development of relative movement equations for a single alumina abrasive grit along the grinding trajectory. The simulation and experimental results obtained from the present study can be helpful to automotive and dies molding industrial applications. Contrary to conventional dry grinding, it has been amply demonstrated that ultrasonic vibration assisted grinding with optimized frequency and amplitude may be a novel route for such exercise.

Since the present investigation relates to "difficult-to-cut" material like AISI D2 tool steel, the benefits of UVADG in terms of chip morphology, temperature field, grinding force, equivalent stress, and strain parameters are of importance for engineering application. These parameters have been established through this work. The unique novelty of the present work is that it has attempted to bridge the above research gap, and it offers an

improvement of our understanding of single grit ultrasonic vibration assisted dry grinding of “difficult-to-cut” steel like AISI D2 tool steel.

4.1 Finite element analysis modelling approach

4.1.1 Geometrical modelling of single alumina grit

The distinct alumina abrasive grits arbitrarily diffuse on the periphery of the grinding wheel. The kinematics of activity among the grits and on the surface of the workpiece is considerably complicated. Mathematical statistics have been adopted for the alumina abrasive grit to obtain the geometrical parameters of the equivalent alumina abrasive grit. The alumina abrasive wheel commonly used for the grinding of tool steels due to its availability and low cost. Some past research groups have used a white light interferometer to estimate the surface topography of alumina wheel with various grit size [250] [251] and it has been seen that the alumina abrasive grit can be interpreted as cone shape with nose radius as shown in Figure 4.1. In this present study, the alumina abrasive grit (grit size #60) is used for FEA modelling analysis according to the parameters of Table 4.1. The details of mathematical parameters [250], thermal-mechanical properties of alumina abrasive grit [189] are presented in the Table 4.1.

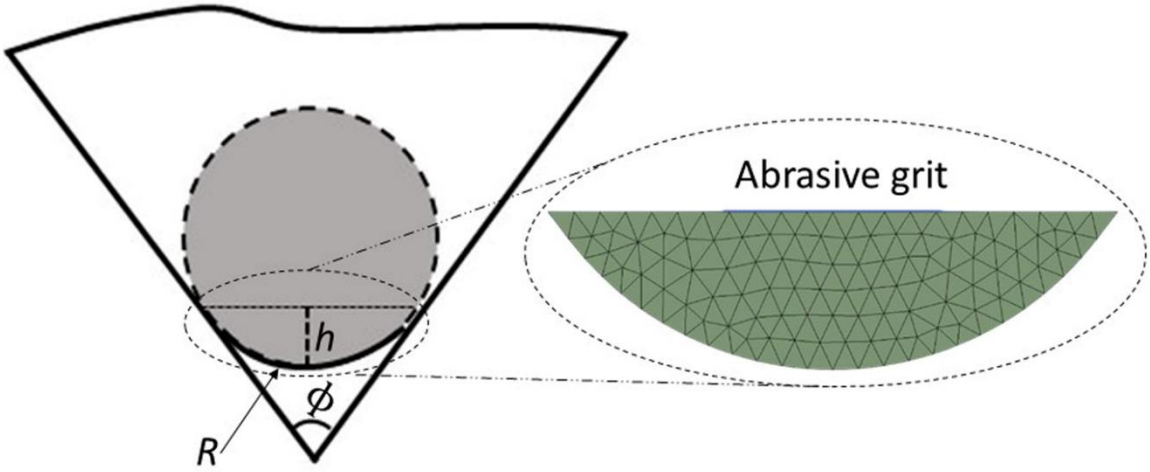

Figure 4.1 Equivalent cone shape with nose radius of alumina abrasive grit

Table 4.1 Mathematical parameters and thermal-mechanical properties of alumina abrasive grit [250] [189]

Mathematical parameters of abrasive grit (#60 grit size)	
Cone angle, ϕ (°)	73.74
Nose radius, R (μm)	41.61
Protrusion height, h (μm)	20
Thermal-mechanical properties of alumina abrasive grit	
Thermal conductivity, K (W/mK)	37
Specific heat capacity, C_p (J/kgK)	880
Young's modulus, E (GPa)	530
Poisson's ratio, v	0.2
Density, ρ (kg/m^3)	4000

4.1.2 Mathematical model for kinematic of abrasive grit in CDG and UVADG

It is essential to investigate the movement of abrasive grit and workpiece for examining the mechanism of UVADG. In UVADG, there are three kinds of motions: grinding wheel speed (V_c), worktable feed rate (V_w) and speed of the ultrasonic vibration along the longitudinal feed direction (V_{ug}) as presented in Figure 4.2. Assuming an angular speed (ω), grinding wheel diameter (D) and wheel speed (V_c) can be written as below equation (4.1):

$$V_c = \frac{D}{2} \times \omega \tag{4.1}$$

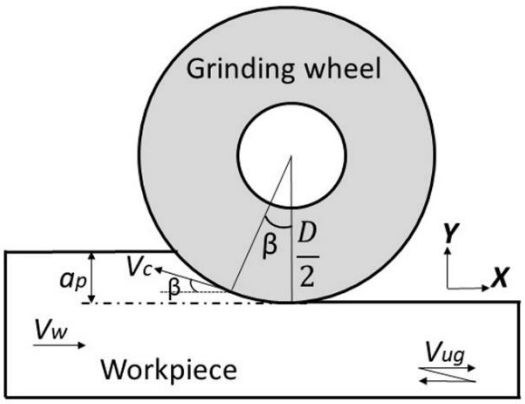

Figure 4.2 Various ultrasonic vibration assisted grinding parameters

abrasive grit speed (V_c) is divided into horizontal (V_{c_x}) and vertical (V_{c_y}) segments, as following equation (4.2) and (4.3):

$$V_{c_x} = V_c \times \cos\beta = V_c \times \cos(\omega \times \tau) \quad (4.2)$$

$$V_{c_y} = V_c \times \sin\beta = V_c \times \sin(\omega \times \tau) \quad (4.3)$$

Where, β is an angle subtended at the centre of the abrasive wheel and workpiece cutting arc during time (τ). When the abrasive grit is down on the circumference of the grinding wheel at that time (τ) is zero.

To achieve a relative speed of abrasive grit with respect to the workpiece, it is assumed that the grit moves against the workpiece but in the opposite direction (V_{fs} = -V_w) rather than a workpiece moving against abrasive grit.

Thus, the abrasive grit relative speed (V_{cr}) is divided into horizontal (V_{cr_x}) and vertical (V_{cr_y}) segments, as following equation (4.4) and (4.5):

$$V_{cr_x} = V_{c_x} + V_{fs} = \frac{D}{2} \times \omega \times \cos(\omega \times \tau) + V_{fs} \quad (4.4)$$

$$V_{cr_y} = V_{c_y} = \frac{D}{2} \times \omega \times \sin(\omega \times \tau) \quad (4.5)$$

Upon integration of equation (4.4) and (4.5) with boundary conditions abrasive grit is at origin (τ =0). The horizontal (S_x) and vertical (S_y) distances of single abrasive grit can be written as:

$$S_x = \frac{D}{2} \times \sin(\omega \times \tau) + V_{fs} \times \tau \quad (4.6)$$

$$S_y = \frac{D}{2} - \frac{D}{2} \times \cos(\omega \times \tau) \quad (4.7)$$

Assuming that time duration for movement of abrasive grit accompanying the cutting curvature is τ'. Thus, S_x and S_y are relative horizontal and vertical distances respectively of the abrasive grit in time duration τ'. Further, the vertical distance is equivalent to downfeed (a_p). $V_{fs} \times \tau$' is abrasive grit insertion in the surface of workpiece in the same direction as table feed rate.

In the UVAG mode, ultrasonic speed and relative horizontal component speed can be added. Assuming vibration amplitude is constant while grinding of the workpiece longitudinally. The horizontal vibration amplitude as following equation (4.8):

$$A_x = A_{ug} \times \sin(2\pi f_{ug} \tau) \quad (4.8)$$

Where, A_{ug} and f_{ug} represent the amplitude and frequency of ultrasonic vibrations, respectively. The ultrasonic vibration speed along the longitudinal feed direction, as following equation (4.9):

$$V_{ug} = A_{ug} \times 2\pi f_{ug} \times \cos(2\pi f_{ug} \tau) \quad (4.9)$$

And net relative horizontal and vertical speed of abrasive grit can be written as following equation (4.10) and (4.11):

$$V_{cr_x} = V_c \times \cos\left(\frac{2V_c}{D} \times \tau\right) + V_{fs} + 2A_{ug}\pi f_{ug} \times \cos(2\pi f_{ug}\tau) \tag{4.10}$$

$$V_{cr_y} = V_c \times \sin\left(\frac{2V_c}{D} \times \tau\right) \tag{4.11}$$

Again, upon integration of equations (4.10) and (4.11) and considering the boundary condition same as above, the relative horizontal and vertical distance components can be written as following equation (4.12) and (4.13):

$$S_x = \frac{D}{2} \times \sin\left(\frac{2V_c}{D} \times \tau\right) + V_{fs} \times \tau + A_{ug} \times \sin(2\pi f_{ug}\tau) \tag{4.12}$$

$$S_y = \frac{D}{2} - \frac{D}{2} \times \cos\left(\frac{2V_c}{D} \times \tau\right) \tag{4.13}$$

Further, the abrasive wheel diameter is large in comparison to the downfeed. So, the contact length (l_c) can be assumed as a straight line in conventional surface grinding, as shown in the

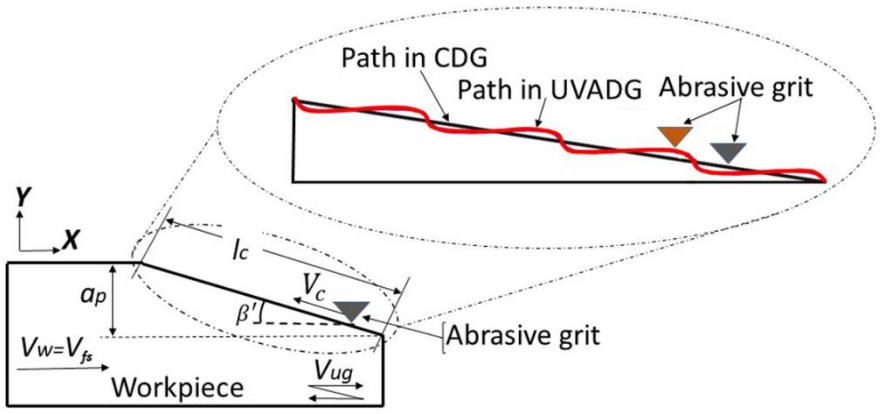

Figure 4.3 Straight line contact length and path of single abrasive grit in CDG and UVADG modes

Figure 4.3. Accordingly, an angle subtended at the centre of the abrasive wheel presented by equation (4.14) can be estimated as an inclination angle (β') for the line of contact presented by equation (4.15).

$$\beta = \cos^{-1}\left(\frac{\frac{D}{2} - a_p}{\frac{D}{2}}\right) \tag{4.14}$$

$$\beta' = \sin^{-1}\left(\frac{a_p}{l_c}\right) = \sin^{-1}\left(\frac{a_p}{\sqrt{(a_p) \times D}}\right) \tag{4.15}$$

By a worktable feed rate transfer to abrasive grit and an assumption of straight-line contact length. The abrasive grit's speed and distances components in the *X* and *Y* direction for CDG can be written as a present by equations (4.16 - 4.19), respectively.

$$V_{cr_x} = V_c \times \cos(\beta') + V_{fs} \tag{4.16}$$

$$V_{cr_Y} = V_c \times \sin(\beta') \tag{4.17}$$

$$S_x = \left(V_c \times \cos(\beta') + V_{fs}\right) \times \tau \tag{4.18}$$

$$S_y = (V_c \times \sin(\beta')) \times \tau \tag{4.19}$$

In case of UVADG, the abrasive grit's speed and distances components in the *X* and *Y* directions can be written as a present by equations (4.20 - 4.23), respectively.

$$V_{cr_x} = V_c \times \cos(\beta') + V_{fs} + 2A_{ug}\pi f_{ug} \times \cos(2\pi f_{ug}\tau) \tag{4.20}$$

$$V_{cr_y} = V_c \times \sin(\beta') \tag{4.21}$$

$$S_x = V_c \times \cos(\beta') \times \tau + V_{fs} \times \tau + A_{ug} \times \sin(2\pi f_{ug}\tau) \tag{4.22}$$

$$S_y = (V_c \times \sin(\beta')) \times \tau \tag{4.23}$$

The equations mentioned above of relative movement of abrasive grit in horizontal and vertical directions can be understood as described in Figure 4.3. In the UVADG, the cutting path is not a straight line but a sinusoidal profile due to ultrasonic vibration, while it is a straight line in conventional grinding. Resultantly, the insertion of abrasive grit is sharp, and the retraction is smooth. Therefore, the abrasive grit forms the chip in lesser duration

in UVADG, whereas conventional grinding gives a minor cut even after prolonged ploughing and rubbing action.

Grinding settings implemented for FEA are listed in Table 4.2. As stated in

Table 4.4, the value of different parameters and the abrasive grit's distance in the X and Y directions in one vibration period (1/21000 s) are calculated according to the equations (4.18), (4.19), (4.22) and (4.23), respectively. The length of the horizontal projection of the contact lines (L) are calculated using estimated inclination angle (β') as mentioned in equation (15).

Table 4.2 Grinding parameters setting implemented in FEA

Parameters	**Conditions**
Grinding mode	Conventional dry grinding (CDG), Ultrasonic vibration assisted dry grinding (UVADG)
Grinding wheel specification	AA-60-K-5-V6
Diameter of grinding wheel (D)	250 mm
Wheel speed (V_c)	39.42 m/s
Worktable feed rate (V_w)	9 m/min
Depth of cut (a_p)	20, 30 and 40 µm
Vibration frequency (f_{ug})	21 kHz
Vibration amplitude (A_{ug})	50 µm
Vibration period (τ'')	$\frac{1}{21000}\ s$

Table 4.3 The values of abrasive grit distance components S_x and S_y in one vibration period and length of the horizontal projection of the contact lines

a_p (μm)	β'(°)	L (mm)	CDG/UVADG	
			S_x (mm)	S_y (mm)
20	0.5125	2.2358	1.8842	0.0155
30	0.6276	2.7387	1.8842	0.0205
40	0.7247	3.1623	1.8842	0.0237

In one vibration period (1/21000 s), the abrasive grit moves an equal distance relative to the workpiece as that of the CDG, although in this period, the actual cutting time is shortened in UVADG. Hence, the cutting time in the period of the UVADG is significant. The values calculated from the above Equations for different downfeed are presented in Table 4.3.

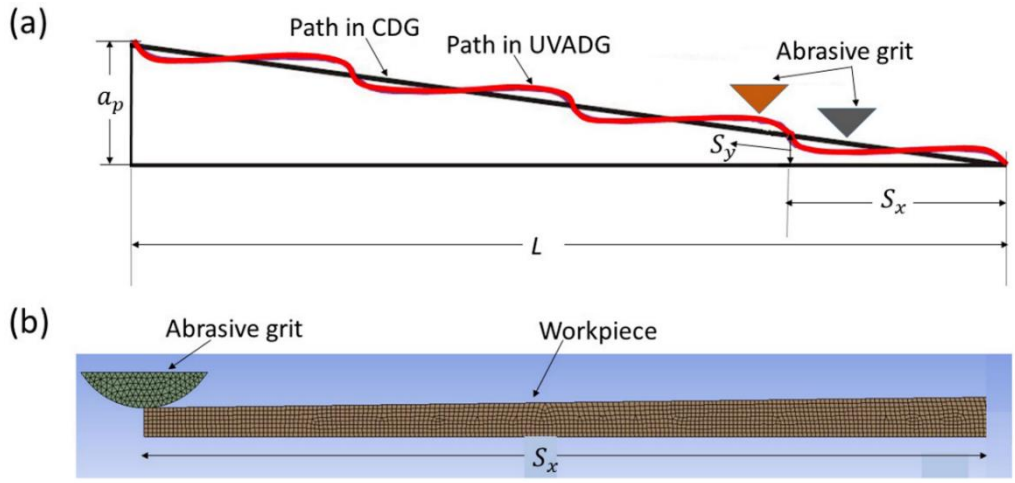

Figure 4.4 (a) Path of abrasive grit in one vibration period, (b) 2D geometrical model of workpiece and abrasive grit for simulation

Figure 4.4 (a, b) illustrates the path of abrasive grit in UVADG and CDG in one vibration period (1/21000 s) and 2D geometrical model of workpiece and abrasive grit for simulation of different grinding modes. In this study, vibration amplitude (A_{ug}) has been taken 50 μm. All other parameters, apart from the vibration amplitude, have been given actual values.

The reason for using such high values of A_{ug} is to ensure that the grit penetrates the workpiece sufficiently. Else the, the penetration will be on the order of microns, necessitating element sizes on the order of microns, resulting in a massive number of elements moving in a single vibration cycle, which is beyond the capability and capacity of our hardware system and FEA software, and the process will be denied.

4.1.3 Deformation and failure laws for workpiece material

AISI D2 tool steel is consider as a workpiece material in the present work. The chemical composition and thermo-mechanical properties of AISI D2 tool steel are presented in

Table 4.4 and Table 4.5. In this study, the Johnson-Cook constitutive model, representing the correlation among flow stress and strain, strain rate, and temperature, has been adopted as the AISI D2 tool steel constitutive model [252] and Johnson-Cook (J-C) model can be expressed by equation (4.24):

$$\sigma = [A + B(\epsilon_P)^n].\left[1 + Cln\left(\frac{\dot{\varepsilon}_p}{\dot{\varepsilon}_o}\right)\right].\left[1 - \left(\frac{T - T_r}{T_m - T_r}\right)^m\right] \quad (4.24)$$

Where, *A*, *B*, *C*, *n* and *m* are indicated as the J-C material constants, and these constants are taken from the published literature [253] and mention in Table 4.6

Table 4.4 Chemical composition of AISI D2 tool steel

Element	**Weight (%)**
Carbon (C)	1.55
Chromium (Cr)	11.80
Silicon (Si)	0.3
Manganese (Mn)	0.40
Molybdenum (Mo)	0.90
Vanadium (V)	0.80
Iron (Fe)	Balance

Table 4.5 Thermo-mechanical properties of AISI D2 tool steel

Material properties	**Values**
Young's modulus, E (GPa)	180
Poisson's ratio, v	0.3
Density, ρ (kg/m^3)	7750
Thermal conductivity, K (W/mK)	21
Specific heat capacity, C_p (J/kgK)	485

Table 4.6 The J-C constitutive model parameters for AISI D2 tool steel [253]

***A* (MPa)**	***B* (MPa)**	***C***	***n***	***m***	***T_m*(ºK)**
1766	904	0.012	0.312	3.38	1733

Where, A: yield stress of the material under reference conditions (MPa), B: strain hardening constant (MPa), n: strain hardening coefficient, C: strengthening coefficient of strain rate, m: thermal softening coefficient, σ: equivalent flow stress. ϵ_p, $\acute{\varepsilon}_p$ and $\acute{\varepsilon}_o$ indicates the equivalent plastic strain, equivalent plastic strain rate, and reference plastic strain rate, respectively. T_w, T_m and T_r indicates workpiece temperature, material melting temperature, and reference ambient temperature, respectively.

The material failure model introduced by Johnson-Cook applying strain as a particular criterion [252]. The Johnson-Cook shear damage criterion is implemented in this investigation as the failure criterion of AISI D2 tool steel. Developed on the equivalent plastic strain, which happens while an integration cycle, the failure happens if $\zeta \geq 1$. The failure parameter (ζ) can be determined through equation (4.25):

$$\zeta = \sum \frac{\Delta \epsilon_P}{\epsilon_f} \tag{4.25}$$

Where, $\Delta\epsilon_P$ is the increment of equivalent plastic strain and ϵ_f is the equivalent strain to failure. ϵ_f expressed by the equation (4.26):

$$\epsilon_f = [D_1 + D_2\, exp(D_3\sigma^*)].\left[1 + D_4 ln\frac{\acute{\epsilon}_p}{\acute{\epsilon}_o}\right].\left[1 - D_5\left(\frac{T_w - T_r}{T_m - T_r}\right)\right] \quad (4.26)$$

Where, σ^*: stress triaxiality factor [σ^*= hydrostatic pressure (σ_p)/von Mises equivalent stress (σ_{mises})], D_1-D_5: failure or damage parameter. The Johnson-Cook damage parameters (D_1-D_5) for AISI D2 tool steel are taken from the published article [254] and shown in the Table 4.7.

Table 4.7 The J-C damage model parameters for AISI D2 tool steel [254]

D_1	D_2	D_3	D_4	D_5
-0.8	1.2	-0.5	0.0002	0.61

In this study, the synergy between abrasive grit and workpiece body interface is represented by coulomb's friction model $(\sigma_{fr} = \mu\sigma_n)$. Where, σ_{fr} and σ_n are frictional stress and normal stress. The isotropic coefficient of friction (μ = 0.3) is fixed corresponding to literature [255].

4.1.4 Boundary condition for FEA simulation

In this study, multiphysics domains such as chip morphology, temperature, and stress strain of single alumina abrasive grit for CDG and UVADG modes cannot performed by experimentally because of the tiny affected region and speedy action of the abrasive grit. The FEA simulation analysis is a helpful tool for the investigation of such types of problems. Ansys Workbench 2020 R1 Explicit dynamics FEA software is used to simulate the CDG and UVADG for AISI D2 tool steel.

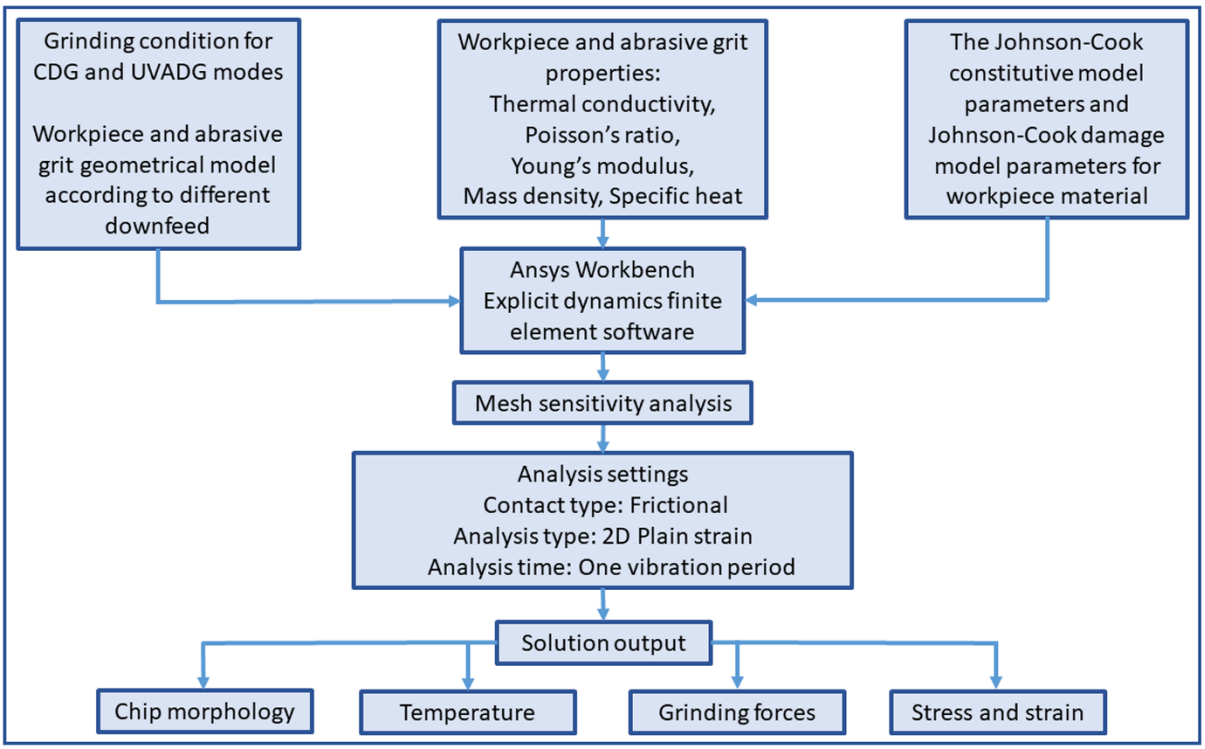

Figure 4.5 Flow chart of FEA simulation for CDG and UVADG process

As listed in Table 4.2, the different grinding parameters and the abrasive grit's speed components in the X and Y direction for CDG and UVADG mode can be calculated by Equations (4.16), (4.17), (4.20) and (4.21), respectively. In order to counter workpiece mobility during cutting by the abrasive grit, the base side and both end sides of the workpiece were considered as fixed support. The contact between abrasive grit and workpiece is considered frictional (μ = 0.3), and the abrasive grit and workpiece body are designating as target body and contact body, respectively. A typical plain strain 2D meshed FEA model of abrasive grit and workpiece as illustrated in Figure 4.4 (b), and the time for the analysis is one vibration period (1/21000 s). In addition, Figure 4.5 presents the flow chart of FEA simulation for different grinding processes. Only one period of ultrasonic vibration was modelled to minimize the calculations time and speed up the modelling speed.

Table 4.8 Mesh sensitivity analysis

Mess size (mm)	Number of nodes and elements		Simulated tangential force (N) in CDG mode
	Nodes	Elements	
0.0032	5572	5095	49.67
0.0027	7502	6937	41.32
0.0023	10026	9363	34.44
0.0020	13039	12278	38.21

In the CDG mode at 40 µm downfeed, the mesh sensitivity analysis was performed to enhance the accuracy of the simulation results of the grinding process as presented in Table 4.8. The mesh size of elements for the workpiece was selected as 0.0023 mm, consisting of 10026 nodes and 9363 elements. At this mess size, the simulated tangential grinding force is 34.44 N, which is closest to the experimental result of tangential grinding force (31.98 N).

4.2 Experimental procedure

An experimental study of single alumina abrasive grit grinding was designed and performed to validate the FEA model and the reliability of the simulated outcomes. Grinding forces during the single alumina abrasive grit in CDG and UVADG modes were measured and compared with simulated results. The details of the experimental procedure have been already discussed in Chapter 3 and Section 3.2.

4.3 Results and discussion

4.3.1 Simulation of grinding chip morphology

In the grinding, mainly three stages of material deformation when an abrasive grit interacts on the work surface that is rubbing, ploughing, and chip cutting. The simulation of three sta1ges while surface grinding of AISI D2 tool steel with single alumina abrasive grit is

illustrated schematically in Figure 4.6. Further, Figure 4.6 (a) shows the rubbing stage appears at a comparatively lower grit penetration, and material removal is negligible. However, friction is apparent in this stage due to elastic deformation near the nascent ground surface. Since the grit penetration progresses, the ploughing stage is begun, through which plastic deformation occurs on the workpiece, and the ridge is formed on the ground surface though the rate of material removal remains negligible, as presented in Figure 4.6 (b).

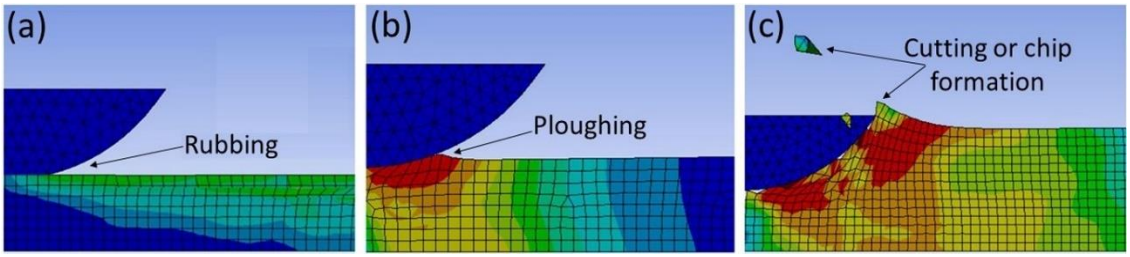

Figure 4.6 The different simulated grinding regimes under single alumina abrasive grit

It can be observed that, the material on the surface of the workpiece cannot be detached during rubbing and ploughing regimes of single grit grinding owing to the lower grit penetration less than the critical chip thickness generation [256]. Lastly, as higher grit penetration is obtained, the critical chip thickness generation, a microchip is generated subsequently and released from the surface of the workpiece, as illustrated in Figure 4.6 (c). Therefore, it can be observed that if the abrasive grit penetration is smaller than the critical chip thickness generation, then the abrasive grit simply rubs and ploughs on the surface of a workpiece, and there is no chip generation. For the purpose of a better interpretation of the UVADG process, simulation of grinding chips under CDG and UVADG modes at different downfeed performed and compared the chip morphology (refer to Figure 4.7). In CDG mode, the twisted long ribbon type grinding chips were generated (refer to Figure 4.7 (a, c, e)) due to the ploughing action taking place between the workpiece

surface and alumina abrasive grit, which also includes comparatively higher grinding forces (refer to Figure 4.9). The above mentioned event has also been validated by the published literature [257]. Figure 4.4 (a) shows the interaction of abrasive grit and workpiece under UVADG mode at the start of the abrasive grit relative movement. Therefore, it is feasible to shift worktable feed rate of workpiece to the abrasive grit. Hence, it is observed in the initial half ultrasonic vibration period, the direction of vibration and shifted relative worktable feed rate is opposite, and the abrasive grit disengage from the sample and goes slightly apart from the sample. Though, in the following half vibration period, the vibration direction and shifted relative worktable feed rate is same and abrasive grit insertion is sharp into the workpiece, which results in minor rubbing and ploughing action in UVADG mode,

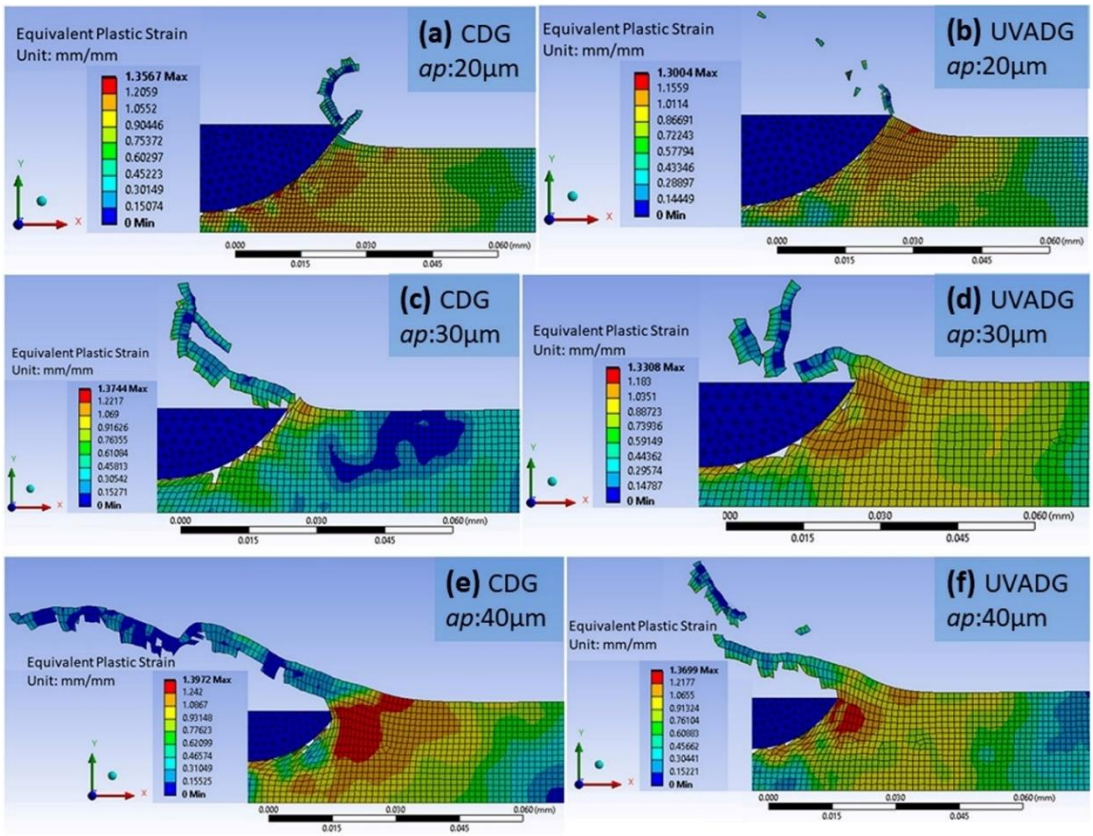

Figure 4.7 Grinding chips obtained at different downfeed under CDG and UVADG modes

as presented in Figure 4.7 (b, d, f). As illustrated in Figure 4.7 (b, d, f), the grinding chips under UVADG mode are much shorter and straighter than CDG mode at all respective downfeed. The published literature has also confirmed the above-mentioned event [26]. These chips are produced by discontinuous shearing action, and this is possibly because of the retention of sharper abrasive grit [258], which is also represented the lower grinding forces obtained in the case of UVADG mode (refer to Figure 4.9). The investigation of chip morphology shows toward the ability of UVADG mode in enhancing the grinding performance of AISI D2 tool steel.

4.3.2 Grinding temperature field simulation

One of the most critical parameters in the grinding process is the temperature distribution in the workpiece. The high grinding temperature can affect the surface integrity of finished sample in terms of change in microhardness and microstructure, oxidation (burring marks) on the ground surface, and induction of the tensile residual stress, which reduces the fatigue life, corrosion, and erosion resistance, and if workpiece material is not sufficiently ductile then induction of residual stress and subsurface cracks [259] [260] [261]. Therefore, grinding temperature simulation and assessment is essential during inline production. The simulated temperature results presenting the temperature distribution fields of the workpiece obtained at variable downfeed during CDG and UVADG modes are illustrated in Figure 4.8. At 20 µm downfeed, the difference between maximum grinding temperature obtained during CDG and UVADG mode is 28.61%, reducing to 24.94% at downfeed 30µm and 21.3% at downfeed 40 µm. Hence, as the downfeed increases, the difference between the maximum grinding temperature during CDG and UVADG mode reduces. During UVADG mode, the workpiece

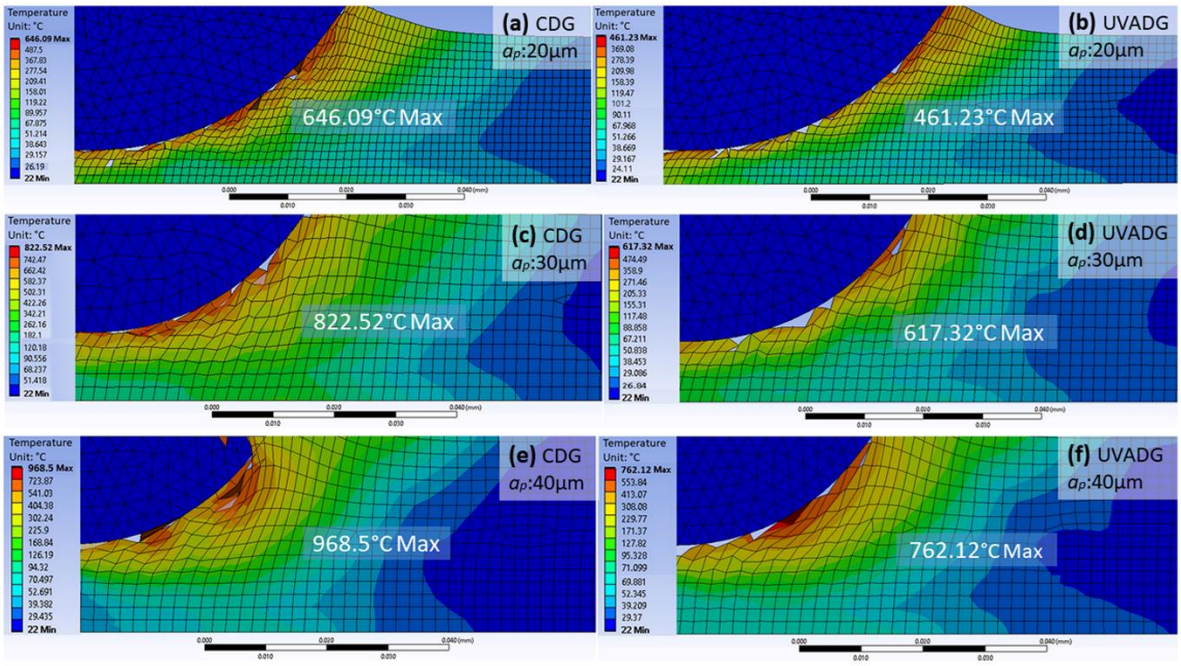

Figure 4.8 Temperature field obtained under CDG and UVADG modes at different downfeed

surface separates from the abrasive grit within per cycle of ultrasonic vibration. Such discontinuous contact reduces the total time for heat conduction between the workpiece and abrasive grit. Resulted in effective cooling in the contact zone by convective heat transfer to the environment [262]. Therefore, a decreasing trend in grinding temperature was obtained during UVADG as followed by CDG mode (refer to Figure 4.8).

4.3.3 Experimental and simulated grinding force

Figure 4.9 shows the experimental and simulated grinding forces results in CDG and UVADG modes for AISI D2 tool steel. As presented in Figure 4.9 (a, b), the tangential grinding force (F_t) and normal grinding force (F_n) is increased with the increase of the downfeed in both grinding modes. As downfeed increases, there will be an improvement in the plastic deformation and material removal, yielding higher grinding forces. Compared to the CDG mode, F_t and F_n grinding forces are further reduced in UVADG mode due to the intermittent cutting action of abrasive grit. Therefore, an intermittent cutting action in

UVADG mode extends the noncutting time of the abrasive grit, which reduces the grinding forces. In UVADG mode, the ultrasonic vibration makes the grinding forces oscillate over a broad range; therefore, the average grinding forces were considered in this study.

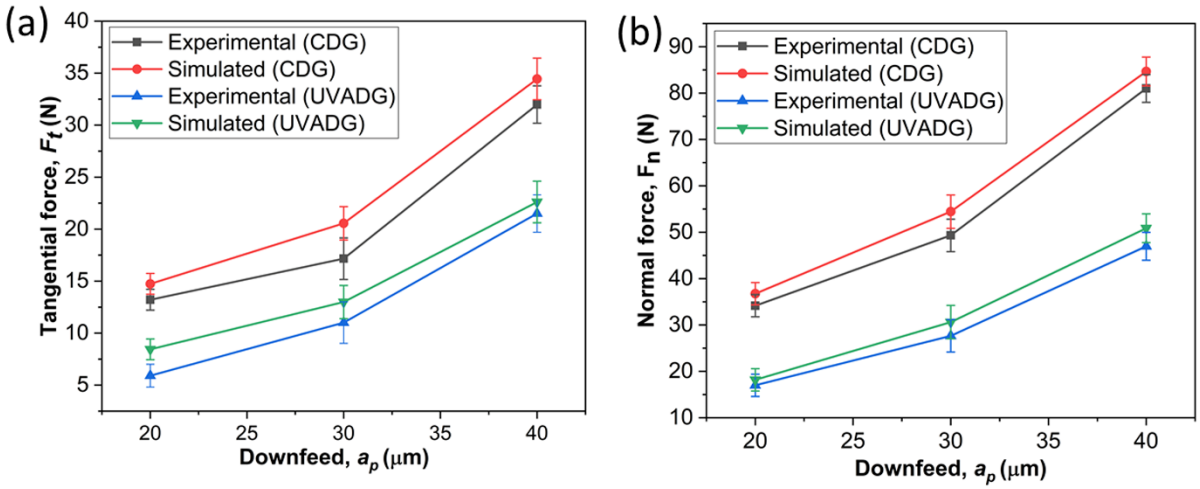

Figure 4.9 Experimental and simulated grinding forces at different downfeed under CDG and UVADG modes

The maximum relative percentage error between experimental and simulated grinding force is below 9% at 40 μm downfeed. However, the experimental values of grinding force lower than the simulation values of the grinding force at all respective downfeed. This happens due to the absolute downfeed less than the desired value in an experimental study. Data interpretation revealed that the F_t and F_n grinding force were decreased by 32.77% and 42.01% in UVADG than CDG mode in experimental condition, while 34.41% and 39.91% in UVADG than CDG modes in simulation at 40μm downfeed. The decrease in F_t and F_n grinding force was obtained during UVADG mode because of the decrease in the frictional

force between the abrasive grit and workpiece seen as a result of pulsating machining characteristic of the abrasive grit [263].

4.3.4 Equivalent von-Mises stress and equivalent plastic strain

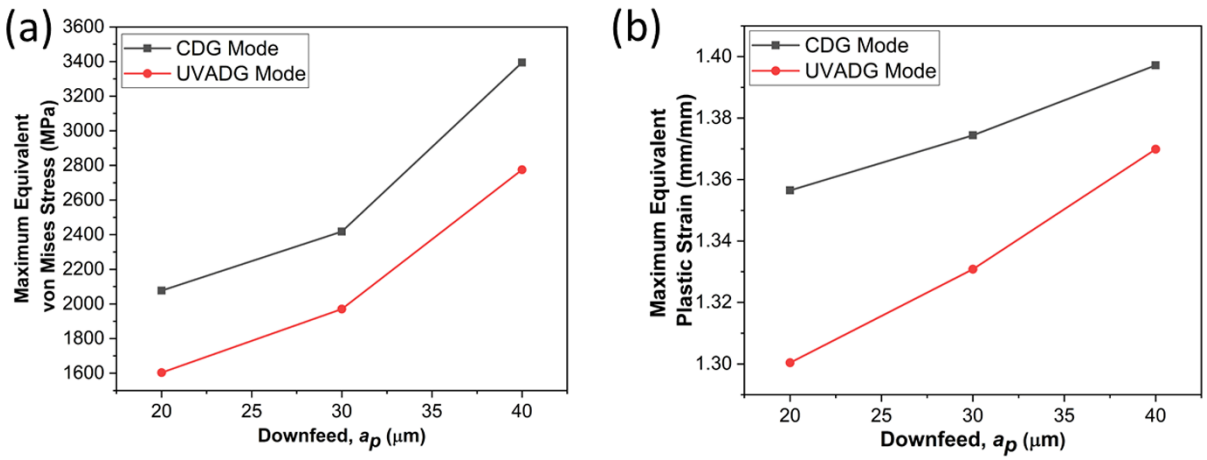

Figure 4.10 Effect of downfeed on (a) Maximum equivalent von Mises stress, (b) Maximum equivalent plastic strain upon single alumina grit in CDG and UVADG modes

Figure 4.10 presents the simulated maximum equivalent von Mises stress and maximum equivalent plastic strain of ground sample at different downfeed under CDG and UVADG modes. The von Mises stress is a criterion for yielding, generally applied for metals. It states that yielding will appear in an object if the stress components working on it are larger than the criterion. In the stress-strain curve of material, the permanent deformation is called plastic deformation after yielding point, and the equivalent plastic strain is the total strain energy of this plastic deformation value on a material [264]. In the actual grinding, the higher grinding forces on the workpiece could result in surface and subsurface microcracks and poor surface integrity. Hence, the stress and strain distribution in the ground workpiece should be studied. The downfeed usually has a significant impact on equivalent von Mises stress and equivalent plastic strain during CDG and UVADG modes. Figure 4.10 (a) shows the maximum equivalent von Mises stresses at 20, 30, and 40 μm downfeed were 2077, 2417.19, and 3394.6 MPa in CDG mode, while 1603.2, 1970.4, and 2775.1 MPa in

UVADG mode, respectively. In compared to the CDG mode, the maximum equivalent von Mises stresses were further decreased in UVADG mode due to the intermittent cutting action of abrasive grit. The reduction in the equivalent von Mises stresses in UVADG mode, which reduces the grinding forces. Figure 4.10 (b) indicates the maximum equivalent plastic strain induced in the workpiece. The maximum equivalent plastic strain at 20, 30, and 40 µm downfeed were 1.3565, 1.3744, and 1.3972 mm/mm in CDG mode, while 1.3004, 1.3308 and 1.3699 mm/mm in UVADG mode, respectively. Therefore, the CDG mode has induced higher equivalent plastic strain than UVADG mode at all downfeed, which results in higher thermo-mechanical load upon the workpiece in CDG mode. Besides, greater heat generation and higher temperature upon the ground workpiece in CDG than UVADG mode. This investigation shows UVADG mode has the least plastic damage on the ground surface at all the downfeed, which may benefit the surface integrity of the ground component.

4.4 Conclusions

The present work examines the simulation of grinding chip morphology, temperature field, grinding force, and equivalent von Mises stress and equivalent plastic strain in single alumina abrasive grit grinding of AISI D2 tool steel with variable downfeed upon CDG and UVADG modes. The simulated grinding force result was validated experimentally. The following conclusions may be drawn:

- At all respective downfeed, significantly shorter and straighter grinding chips was produced under UVADG mode due to discontinuous micro-shearing action. Grinding chip morphology shows the ability of UVADG mode to enhance the grindability of AISI D2 tool steel.

- The minimum grinding temperature was observed under UVADG as followed by CDG mode at all respective downfeed caused by a small contact time between the abrasive grit and workpiece and subsequent convective cooling of the abrasive grit.
- The maximum relative percentage error between experimental and simulated grinding force is below 9% at 40 μm downfeed. The F_t and F_n were decreased by 32.77% and 42.01% in UVADG experimentally, while 34.41% and 39.91% in UVADG than CDG mode in simulation, respectively.
- The lower maximum equivalent von Mises stresses were obtained in UVADG mode due to the intermittent cutting action of abrasive grit, which helps to minimize the grinding force. Moreover, UVADG mode has produce a least plastic damage on the ground surface, which may benefit the surface integrity of the ground component.